coatings

MDPI

Article

Investigations of Thermal Stability and Spectroscopic Features of Sm^{3+} Doped Strontium Aluminate Glasses

Pengfei Li [1,2,*], Xiaoyan Zhang [1,2,3], Jinrong Zhang [1,2], Xiwei Qi [2,3,4,*] and Xin Liu [5,*]

[1] School of Materials Science and Engineering, Northeastern University, Shenyang 110819, China; xyaaa2005@163.com (X.Z.); coco_jr_zhang@163.com (J.Z.)
[2] School of Resources and Materials, Northeastern University at Qinhuangdao, Qinhuangdao 066004, China
[3] Key Laboratory of Dielectric and Electrolyte Functional Material, Qinhuangdao 066004, China
[4] College of Metallurgy and Energy, North China University of Science and Technology, Tangshan 063210, China
[5] State Key Laboratory of Hydraulic Engineering Simulation and Safety, Tianjin University, Tianjin 300072, China
* Correspondence: lipengfei@neuq.edu.cn (P.L.); qixiwei@mail.neu.edu.cn (X.Q.); lx_2020@tju.edu.cn (X.L.)

Abstract: In the present work, a series of Sm^{3+} doped transparent strontium aluminate glasses with the composition Al_2O_3-(3-x)SrO: xSm^{3+} (x = 0, 0.01, 0.03, 0.06, 0.1, 0.2) were fabricated by a containerless process using an aerodynamic levitation furnace. The structural characteristics, density, Vicker's hardness, and thermal and spectroscopic behaviors of these glasses were investigated. All the glasses exhibit excellent thermal stabilities ($T_g \geq 792$ °C) and the glass-forming ability is enhanced with the increasing content of Sm^{3+}. The emission spectra recorded under an excitation of 404 nm show four emission transitions as a result of $^4G_{5/2}$ translated to the lower states of $^6H_{5/2}$, $^6H_{7/2}$, $^6H_{9/2}$, and $^6H_{11/2}$, and a bright orange-reddish luminescence can be observed in Al_2O_3-(3-x)SrO: xSm^{3+} glasses. The high thermal stability, good glass-forming ability and excellent hardness provide new options for the development of visible orange-reddish lasers and smart photoluminescent glass coating materials.

Keywords: luminescent glass; containerless; Sm^{3+} doped; thermal stability; CIE co-ordinates

check for updates

Citation: Li, P.; Zhang, X.; Zhang, J.; Qi, X.; Liu, X. Investigations of Thermal Stability and Spectroscopic Features of Sm^{3+} Doped Strontium Aluminate Glasses. *Coatings* **2022**, *12*, 3. https://doi.org/10.3390/coatings12010003

Academic Editor: Anil K. Battu

Received: 26 November 2021
Accepted: 16 December 2021
Published: 21 December 2021

1. Introduction

Oxide glasses containing luminescent rare-earth (RE) ions have been widely investigated due to their excellent photoluminescence properties, outstanding optical properties and high thermal and chemical stabilities. Numerous applications as functional photonic devices [1–3] and smart glass coating materials [4,5] have been carried out in these glasses. However, the spectroscopic properties of RE ions in these glasses are susceptible to the surrounding environment and the distribution of ions doped in the glassy matrix [6]. Aluminate-based materials have been widely concerned for their high stability, quantum efficiency, high transparency in the UV-Vis range and decent mechanical property [4,5,7–9]. Studies have shown that the presence of alkaline earth is of great benefit to the chemical resistance of the glass substrate [10], and alkaline earth aluminate-based luminescent materials have been extensively applied as host materials. It was noticed that the Al_2O_3-SrO system can form solid solutions with various metal oxides, which results in certain modifications in crystal structure and optical properties [11]. Therefore, in-depth study of RE-doped Al_2O_3-SrO glassy systems would promote the understanding of its multifunctional properties, such as the thermal, mechanical and optical properties.

Sm^{3+} is well known as an important rare earth activator that exhibits unique properties, such as strong reddish-orange emission due to its $^4G_{5/2} \rightarrow {}^6H_J$ (J = 5/2, 7/2, 9/2, 11/2) transition, high quantum and luminescence efficiencies. Sm^{3+} ions doped glasses, such as single alkali and mixed alkali fluoro tungsten tellurite glasses [12], sodiumfluoro-phosphate glasses [13], Li_2O-MO-B_2O_3 (M = Mg/Ca/Sr/Ba) glasses [14], lead fluoro-borophosphate glasses [15], borate glasses [16], etc., have been investigated for decades to explore their structural, spectroscopic and luminescent properties. Numerous applications of Sm^{3+} doped glasses in the field of visible solid state lasers, optical memory devices, submarine communication and display devices have been developed [17–19]. Predictably, the introduction of Sm^{3+} ions into the Al_2O_3-SrO glassy system is of great significance for developing new optical devices with specific utility and enhanced performance.

In this work, we focused on Sm^{3+} doped Al_2O_3-SrO glasses to explore the effect of samarium concentration on the structural, mechanical and thermal stability, as well as the absorption and emission spectra of these glasses. The difference between the crystallization temperature T_x and glass transition temperature T_g (i.e., ΔT) was measured to evaluate the glass-forming ability. Additionally, the nephelauxetic effect β and bonding parameters δ were analyzed from the absorption spectral features, from which the nature of Sm^{3+}-ligand bond in the glass can be identified. Moreover, based on the emission spectra, the $^4G_{5/2} \rightarrow {}^6H_{7/2}$ (607 nm) transition exhibits the maximum intensity, indicating that the Sm^{3+} doped Al_2O_3-SrO glasses (namely Al_2O_3-(3-x)SrO: xSm^{3+} glasses) show a bright orange-reddish emission under an UV source. In addition, a moderate amount of Sm^{3+} doping can enhance the Vicker's hardness (with a value of 7.03 GPa) and thermal stability (with high T_g values of over 792 °C) of these glasses, which provide more options for the manufacture of novel visible orange-reddish lasers and smart photoluminescent glass coatings.

2. Experimental Procedure

Sm^{3+} doped Al_2O_3-(3-x)SrO: xSm^{3+}(x = 0, 0.01, 0.03, 0.06, 0.1, 0.2) luminescent glasses were successfully prepared by a containerless process using an aerodynamic levitation furnace (ALF, Shanghai Institute of Ceramics, Shanghai, China). Stoichiometric amounts of high purity (>99.9%) raw materials of Al_2O_3, SrO and Sm_2O_3 (China New Metal Materials Technology Co., Ltd., Beijing, China) were milled for two hours with ZrO balls using alcohol as a medium. The speed of the ball mill is 200 rpm, and the quality of the ball mill is about 5 times that of the raw material. After being blended well, the mixture of about 1 g was compacted into disks of diameter 10 mm, melted by a CO_2 laser device (ALF, Shanghai Institute of Ceramics, Shanghai, China) and levitated by oxygen gas flow. The samples were kept in a molten state for ~20 s to ensure homogenization. Then, the melts were rapidly cooled down to room temperature by shutting off the laser power, and transparent glassy-spheres with a diameter of approximately 2–4 mm were obtained. Part of the glassy spheres were carefully polished into disks for structural and performance analyses.

The structures of the samples were examined by X-ray diffraction (XRD, Smartlab, Rigaku D/MAX/2500/PC, Tokyo, Japan) analysis. A high-resolution TEM (HRTEM) image and the electron diffraction pattern were observed by transmission electron microscopy (TEM, Tecnai G2 F20, FEI, Phoenix, AZ, USA). Bulk densities of the glasses were measured by the Archimedes method. Vicker's hardness was tested for each sample via a digital hardness tester (MHV-50Z/V2.0, Sctmc, Beijing, China) equipped with a Vickers indenter with an applied load of 500 g for 10 s. Differential thermal analysis (DTA) was obtained by using an Evolution system (Setsys, Setaram, Lyon, France) at a heating rate of 10 °C/min in the temperature range of 600 °C to 1000 °C in an argon atmosphere. Optical absorption spectra in the wavelength range of 300–1800 nm were detected by an UV-Vis spectrometer (Cary5000, Varian, Palo Alto, CA, USA). The luminescence properties and fluorescence decay curves were measured by fluorescence spectrofluorometers (F-7000, Hitachi, Tokyo, Japan, and F-7100, Hitachi, Tokyo, Japan, respectively).

3. Results and Discussion

3.1. Structural Properties

Considering the similar structural characteristics of Al_2O_3-(3-x)SrO: xSm^{3+} glasses, typical XRD patterns of selective x = 0, 0.06 and 0.2 are shown in Figure 1. It can be seen that each sample exhibits a broad diffusive diffraction peak centered at $2\theta \approx 31°$, indicating the amorphous nature of Al_2O_3-(3-x)SrO: xSm^{3+} glasses. In order to obtain a high-resolution image and further confirm the structural characteristics, the HRTEM micrograph and the corresponding electron diffraction pattern of a randomly selected composition of x = 0.03 are captured and shown in Figure 2. It is observed that no significant grains, second phases or residual pores are detected in Figure 2a and only a broad diffuse halo is presented in Figure 2b, which further confirms the complete glassy state of Al_2O_3-(3-x)SrO: xSm^{3+} samples. These results suggest that uniform transparent Al_2O_3-(3-x)SrO: xSm^{3+} glasses could be successfully prepared by a containerless process.

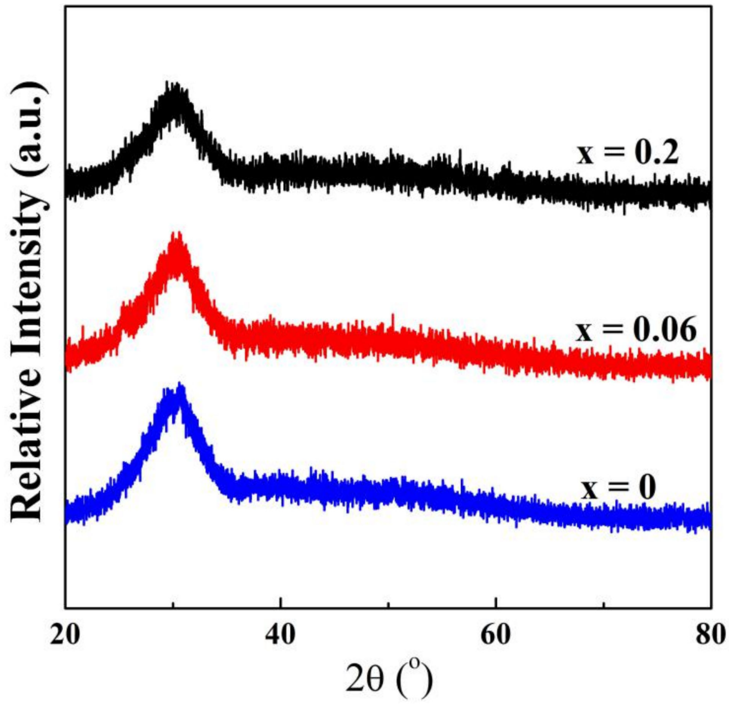

Figure 1. XRD patterns of Al_2O_3-(3-x)SrO: xSm^{3+} (x = 0, 0.06, 0.2) glasses.

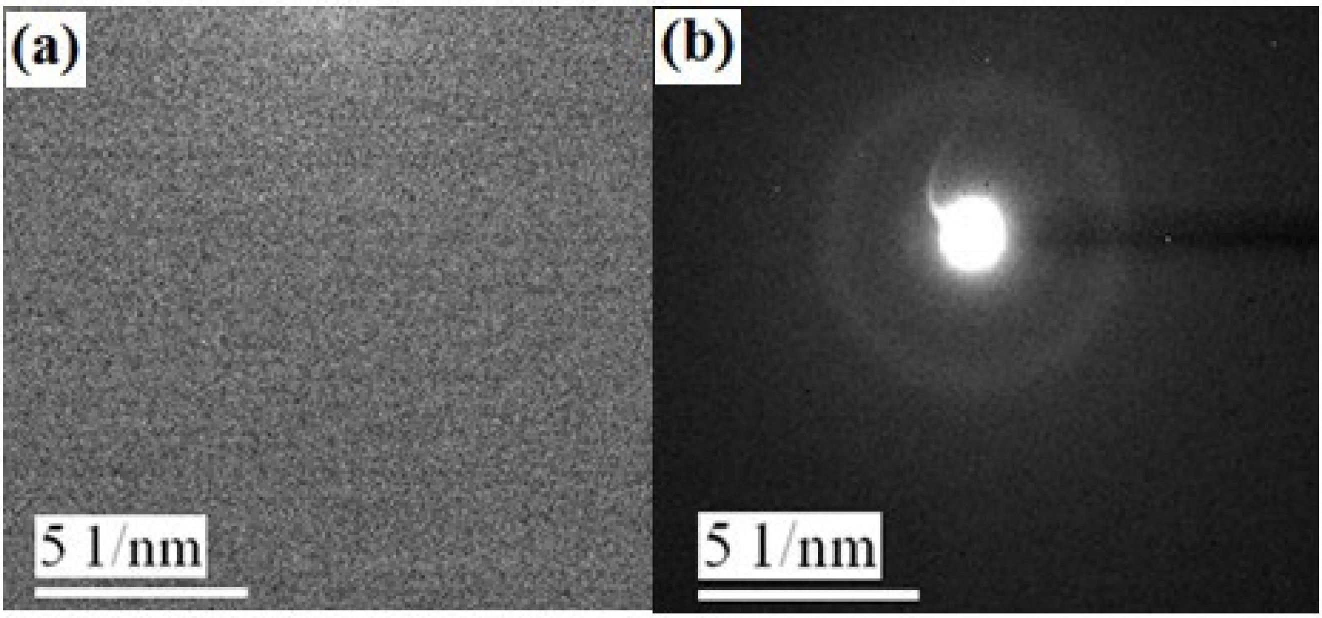

Figure 2. (**a**) HRTEM micrograph; (**b**) the electron diffraction pattern of Al_2O_3-(3-x)SrO: xSm^{3+} glass with x = 0.03.

3.2. Density and Vicker's Hardness

Figure 3 depicts the Vicker's hardness and density (ρ) of Al_2O_3-(3-x)SrO: xSm^{3+} glasses. Both Vicker's hardness and density of the as-prepared glasses increased with rising Sm^{3+} content, with values from 5.01 to 7.03 GPa and 3.99 to 4.12 g/cm^3 for x = 0 to 0.2, respectively. The density of Sm_2O_3 (8.35 g/cm^3) is larger than the SrO (4.70 g/cm^3), content, and hence, the substitution of the lighter SrO by the heavier Sm_2O_3 can lead to an increase in density. In addition, the ionic radius of Sm^{3+} (96 pm) is slightly smaller than Sr^{2+} (118 pm). The replacement of Sr^{2+} ions by Sm^{3+} ions decreases the spatial distance between ions, which is inversely proportional to hardness [20] and results in the rise of Vicker's hardness. The highest value of Vicker's hardness is 7.03 GPa for x = 0.2, which is larger than the reported Sm^{3+} doped oxide glasses [21] and exhibits good potential for mechanical applications.

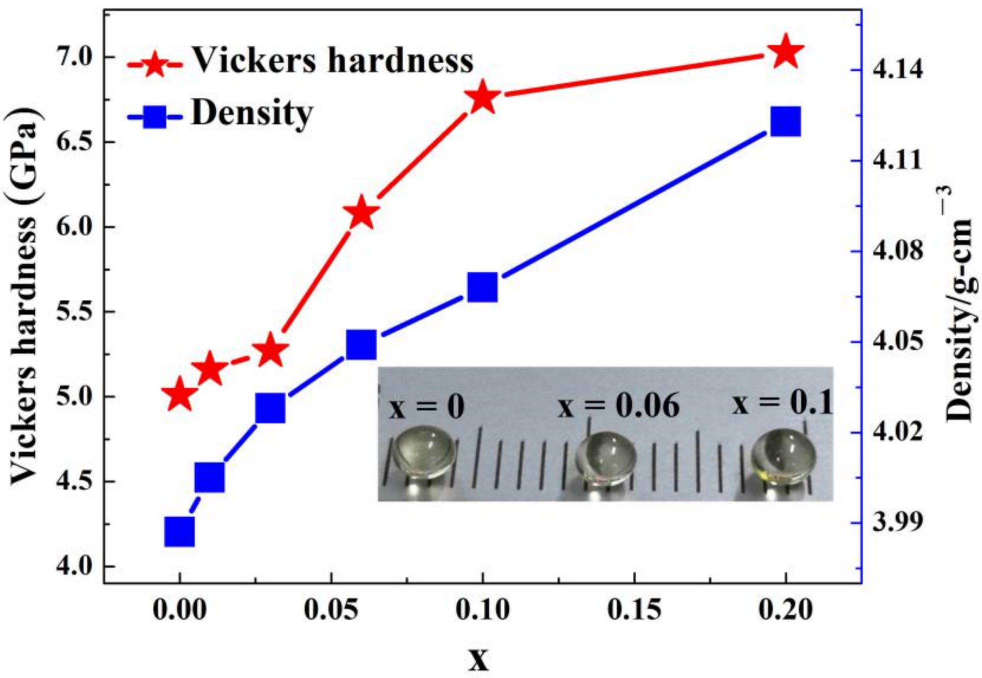

Figure 3. Vicker's hardness and density of Al_2O_3-(3-x)SrO: xSm^{3+}(x = 0, 0.01, 0.03, 0.06, 0.1, 0.2) glasses. The inset photo shows transparent samples of three randomly selected components with x = 0, 0.06, 0.1.

3.3. Thermal Properties

Thermal stability determines the service conditions of glasses. The differential thermal analyses (DTA) curves were measured to study the thermal stability, glass-forming ability and crystallization behavior of Al_2O_3-(3-x)SrO: xSm^{3+} (x = 0, 0.01, 0.03, 0.06, 0.1, 0.2) glasses, as shown in Figure 4. The intersection of tangents overlaid across the endothermic peaks is specified as the glass transition temperature T_g, and the exothermic peak is assigned to the crystallization temperature T_p. The detailed T_g, crystallization onset temperature T_x, crystallization temperatures T_{p1} and T_{p2}, as well as the supercooled liquid region ΔT (defined as $\Delta T = T_x - T_g$), are summarized in Table 1. ΔT has been used to evaluate glass-forming ability, and higher values of ΔT correspond to superior glass-forming ability [22,23]. It can be seen that T_g slightly declines with increasing x, as a sign of thermal stability reduction, which suggests that the substitution of Sm_2O_3 for SrO may weaken the network connectivity of matrix glass. Nevertheless, it can be observed that each T_g of the glasses is still above 792 °C, significantly superior to those Sm^{3+} doped phosphate-based glasses [24], zinc magnesium sulfophosphate glasses [17] and calcium sulfoborophosphate glasses [25], confirming a higher thermal stability. Meanwhile, T_x tends to increase with rising Sm_2O_3

content, which leads to the widening of the supercooled liquid region. For instance, ΔT for x = 0, 0.01 and 0.03 are lower than 60 °C, which means the inferior glass-forming ability of these glasses. When the higher content of Sm_2O_3 is followed, such as x = 0.06, 0.1 and 0.2, the values of ΔT increased significantly and reached 99 °C, 121 °C and 127 °C, respectively. The booming supercooled liquid region ΔT well confirmed the prosperous glass-forming ability when SrO is partially replaced by Sm_2O_3. Therefore, a suitable amount of Sm_2O_3 modified Al_2O_3-SrO glasses exhibit high thermal stability and glass-forming ability, which are of benefit to their applications in coating fields [4].

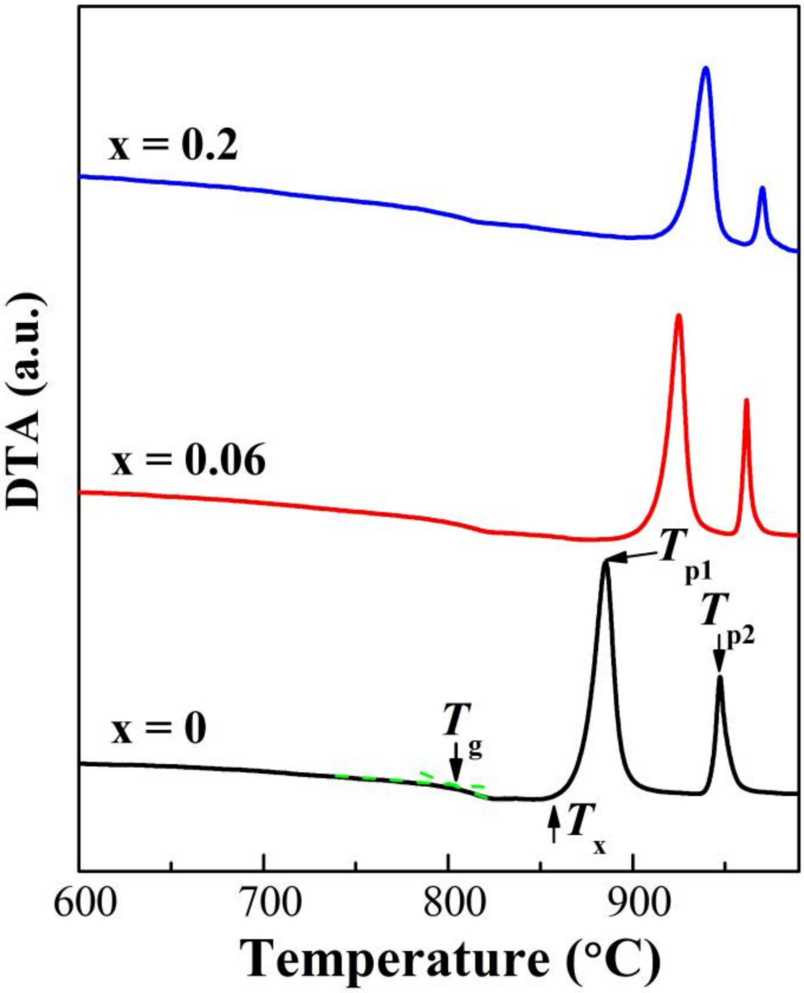

Figure 4. DTA curves of Al_2O_3-(3-x)SrO: xSm^{3+} (x = 0, 0.06, 0.2) glasses.

Table 1. Thermal properties, T_g, T_x, T_{p1}, T_{p2} and ΔT of Al_2O_3-(3-x)SrO: xSm^{3+} (x = 0, 0.01, 0.03, 0.06, 0.1, 0.2) glasses.

x	T_g (°C)	T_x (°C)	T_{p1} (°C)	T_{p2} (°C)	ΔT (°C)
0	804	858	885	947	54
0.01	800	854	884	950	54
0.03	798	854	882	963	56
0.06	798	897	925	962	99
0.1	797	918	938	964	121
0.2	792	919	940	971	127

3.4. Absorption Spectra and Nephelauxetic Effect

Figure 5 presents the absorption spectra of Al_2O_3-(3-x)SrO: xSm^{3+} (x = 0, 0.01, 0.03, 0.06, 0.1, 0.2) glasses in the UV-Vis-NIR region. In the current investigation, all Sm^{3+} ions doped glasses exhibit nearly the same absorption spectra, with several inhomogeneous bands corresponding to the characteristic f-f transitions from the ground state $^6H_{5/2}$ to various excited states. The absorption peaks centered at about 360, 375, 404, 1066, 1214, 1356, 1460 and 1523 nm can be assigned to the $^4D_{3/2}$, $^6P_{7/2}$, $^6P_{3/2}$, $^6F_{9/2}$, $^6F_{7/2}$, $^6F_{5/2}$, $^6F_{3/2}$ and $^6H_{15/2}$ transitions, respectively, similar to those reported in other Sm^{3+} ions doped glasses [26,27]. For the present system, most of the absorption peaks are induced electric dipole contributions with the selection rule $\Delta J \leq 6$ and a few magnetic dipole transitions followed the selection rule $\Delta J = 0, \pm 1$. According to Boehm et al. [28], the absorption bands of Sm^{3+} ion can be divided into two groups: a low-energy group in the NIR region and a high-energy group in the UV-Vis region. The transition $^6H_{5/2} \rightarrow {}^6F_{7/2}$ seems to be stronger in the NIR region, whereas, in the UV-Vis region, the transition $^6H_{5/2} \rightarrow {}^6P_{3/2}$ appears to be the most intense compared with other transitions in the UV-Vis and NIR regions.

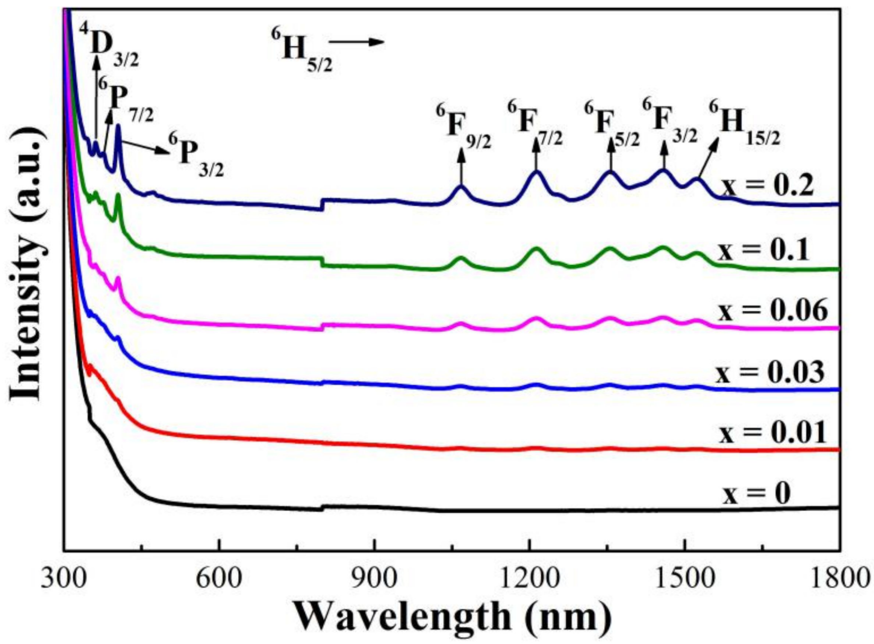

Figure 5. The absorption spectra of Al_2O_3-(3-x)SrO: xSm^{3+} (x = 0, 0.01, 0.03, 0.06, 0.1, 0.2) glasses.

Generally, the nephelauxetic effect results from the expansion of partially filled f-shells and is used to identify the covalency of the RE-O bond in the host matrix [29,30]. To further confirm the absorption transitions of Sm^{3+} ions in the as-prepared samples and investigate the nature of Sm^{3+}-ligand bond in the glass, the nephelauxetic ratio β and bonding parameter δ were evaluated. The nephelauxetic ratio is given by the ratio of the observed wave number for a particular absorption transition of the RE^{3+} ion in the host under investigation (ν_c in cm^{-1}) to the same transition of the aquoion (ν_a in cm^{-1}). Then, the bonding parameter δ can be determined from the average nephelauxetic ratio $\overline{\beta}$ using the following expression [31]:

$$\delta = \left(\frac{1 - \overline{\beta}}{\overline{\beta}} \right) \times 100 \quad (1)$$

The δ can be presented as a positive or a negative value and determined by the ligand field environment, thus implying the corresponding covalent or ionic nature of RE^{3+}-ligand bond. The calculated values of $\overline{\beta}$ and δ for the Al_2O_3-(3-x)SrO: xSm^{3+} glasses are shown in Table 2. The negative δ values reflect the ionic nature of the prepared Sm^{3+}-doped glasses and the ionicity gradually decreases with the increase of Sm^{3+} ions concentration, which indicates that a higher amount of Sm^{3+} results in altering the dominant form of bonding. A similar ionic bonding nature has also been observed in Sm^{3+}-doped zinc fluorophosphate glasses [32], sodium potassiumborate glasses [27] and zinc alumino bismuth borate glasses [33].

Table 2. Band positions of observed ν_c and aqueous solution ν_a (cm^{-1}), Nephelauxetic effect (β) and bonding parameters (δ) of Al_2O_3-(3-x)SrO: xSm^{3+} (x = 0.01, 0.03, 0.06, 0.1, 0.2) glasses.

Transition $^6H_{5/2} \rightarrow$	ν_c **(x = 0.01)**	ν_c **(x = 0.03)**	ν_c **(x = 0.06)**	ν_c **(x = 0.1)**	ν_c **(x = 0.2)**	ν_a **[29]**
$^4D_{3/2}$	27,778	27,778	27,701	27,701	27,701	27,700
$^6P_{7/2}$	26,667	26,667	26,667	26,667	26,525	26,750
$^6P_{3/2}$	24,814	24,752	24,691	24,691	24,691	24,950
$^6F_{9/2}$	9390	9363	9372	9372	9381	9200
$^6F_{7/2}$	8244	8230	8251	8237	8237	8000
$^6F_{5/2}$	7380	7375	7375	7375	7375	7100
$^6F_{3/2}$	6849	6854	6849	6854	6854	6630
$^6H_{15/2}$	6566	6570	6562	6566	6566	6508
$\overline{\beta}$	1.01585	1.01504	1.01459	1.01454	1.01400	-
δ	−1.56021	−1.48135	−1.43759	−1.43296	−1.38035	-

3.5. Photoluminescence Properties

The excitation spectra are often used to extract the efficient luminescence properties and recognize the higher energy levels of Sm^{3+} ions. Figure 6 exhibits the photoluminescence excitation spectra of Al_2O_3-(3-x)SrO: xSm^{3+} glasses in the region of 300–550 nm under the emission wavelength of 607 nm. The excitation bands arising caused by the f-f transitions of Sm^{3+} ions are observed at 316, 344, 360, 375, 404, 420, 470 and 488 nm, corresponding to the transitions from the ground state $^6H_{5/2}$ to $^4P_{3/2}$, $^4D_{7/2}$, $^4D_{3/2}$, $^6P_{7/2}$, $^6P_{3/2}$, $^6P_{5/2}$, ($^4I_{13/2}$ + $^4I_{11/2}$) and $^4I_{9/2}$, respectively [19,34]. Clearly, the highest intensity of the excitation spectra is the $^6H_{5/2} \rightarrow {}^6P_{3/2}$ transition centered at 404 nm, which is selected as an excitation source for the measurement of emission spectra.

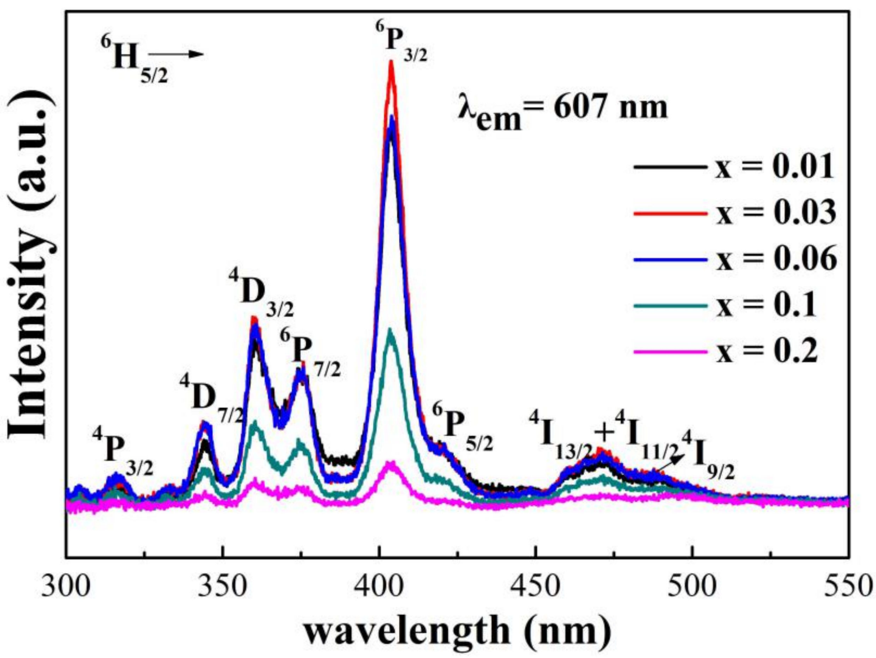

Figure 6. Photoluminescence excitation spectra of Al_2O_3-(3-x)SrO: xSm^{3+} (x = 0, 0.01, 0.03, 0.06, 0.1, 0.2) glasses under an excitation of 607 nm.

Figure 7 shows the emission spectra of Al_2O_3-(3-x)SrO: xSm^{3+} glasses excited at 404 nm ($^6H_{5/2} \rightarrow {}^6P_{3/2}$) within the spectral range 550–750 nm. The emission spectra consist of potential green, orange-reddish and red emission bands centered at 568, 607, 655 and 712 nm. These bands can be assigned to the emission transition $^4G_{5/2} \rightarrow {}^6H_{5/2}$, $^6H_{7/2}$, $^6H_{9/2}$ and $^6H_{11/2}$, respectively, which are similar to the emission characteristics of the other Sm^{3+} doped glasses [13,35]. Among these four transitions, the $^4G_{5/2} \rightarrow {}^6H_{7/2}$ (607 nm) transition exhibits the maximum intensity, indicating that the Sm^{3+} doped Al_2O_3-(3-x)SrO: xSm^{3+} glasses show a bright orange-reddish emission under an UV source. These results are significant for color displays, medical diagnostics and high-density optical data storage [36]. In addition, the photoluminescence intensity relative to $^4G_{5/2} \rightarrow {}^6H_{7/2}$ transition is found to increase with the rising content of Sm^{3+} ion up to x = 0.03, and then a luminescence quenching behavior is observed beyond the critical Sm^{3+} ion concentration of x = 0.03. Generally, the active ions can aggregate with others along with the increasing concentration and result in the cross-relaxation process between Sm^{3+}-Sm^{3+} ions, leading to emission quenching [15].

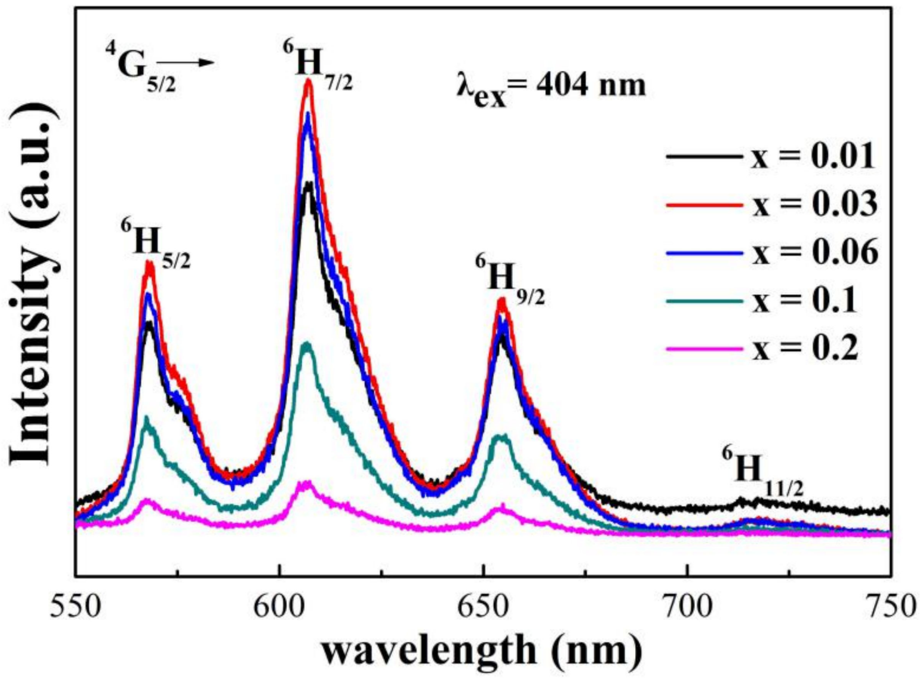

Figure 7. Photoluminescence emission spectra of Al_2O_3-(3-x)SrO: xSm^{3+} (x = 0.01, 0.03, 0.06, 0.1, 0.2) glasses (λ_{ex} = 404 nm).

Information about the decay behaviors and lifetimes of the excited state of rare-earth ions can be provided by analyzing the emission decay curves. The Sm^{3+} emission decay curves of Al_2O_3-(3-x)SrO: xSm^{3+} glasses for $^4G_{5/2} \rightarrow {}^6H_{7/2}$ (607 nm) transition under 404 nm excitation are displayed in Figure 8. It is noticed that the decay curves deviate from the single exponential law and exhibit non-exponential behavior for all glasses. This non-exponential behavior may be attributed to the energy transfer through cross-relaxation between the Sm^{3+} ions in different sites [37]. The non-radiative decay rate can be evaluated experimentally by combining the lifetime measurement. Given that the best fit is obtained by using bi-exponential expression for all the decay curves, as follows:

$$I = I_0 + A_1 e^{\frac{-t}{\tau_1}} + A_2 e^{\frac{-t}{\tau_2}} \quad (2)$$

where I is the luminescence intensity at time t, I_0 is the initial emission intensity, A_1, A_2 are scalar constants obtained from the curve fitting, and τ_1, τ_2 are the lifetimes related to the fast and slow decays. The average values of decay time (τ_{av}) of $^4G_{5/2}$ excited level of Sm^{3+} ions can be calculated as [37,38]:

$$\tau = \frac{A_1\tau_1{}^2 + A_2\tau_2{}^2}{A_1\tau_1 + A_2\tau_2} \tag{3}$$

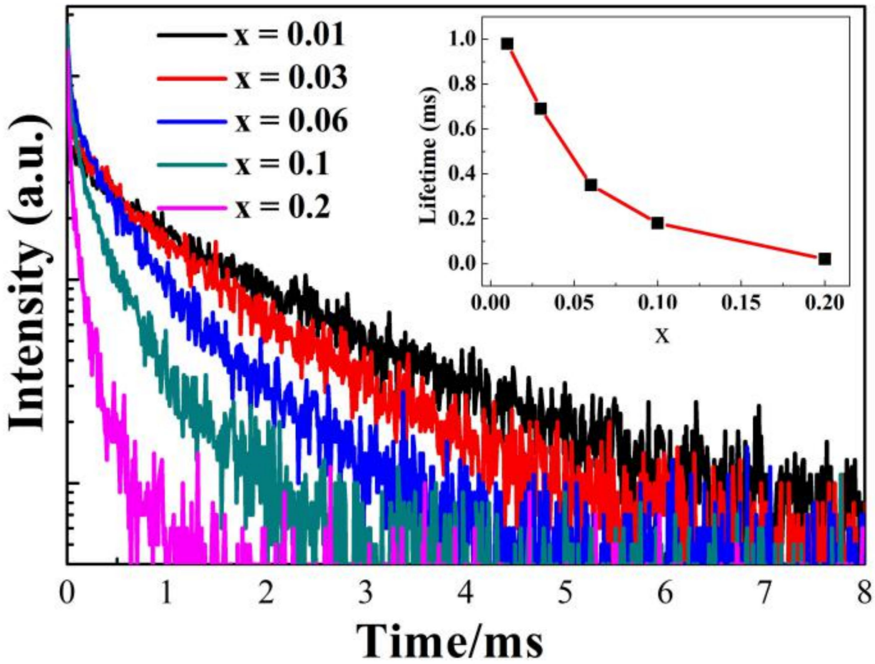

Figure 8. Decay curves and luminescence lifetimes of the $^6H_{7/2}$ emitting level of Sm^{3+} ions inAl_2O_3-(3-x)SrO: xSm^{3+} (x = 0.01, 0.03, 0.06, 0.1, 0.2) glasses.

The calculated τ_{av} values of Sm^{3+}doped Al_2O_3-(3-x)SrO: xSm^{3+} glasses are given in the inset of Figure 8. As shown, the τ_{av} values are found to be 0.98 (x = 0.01), 0.69 (x = 0.03), 0.35 (x = 0.06), 0.18 (x = 0.1) and 0.02 ms (x = 0.2), which are in the order of milliseconds, corresponding to the characteristics of the f $\rightarrow$ f transition of samarium ions [39]. The τ_{av} value decreases with the rising concentration of Sm^{3+} ions. Quenching of the $^4G_{5/2}$ lifetime and the non-exponential nature of the decay curves are the characteristic features for the existence of concentration quenching caused by the energy transfer among Sm^{3+} ions [40].

Finally, the CIE (Commission Internationale Eclairage 1931) chromaticity diagram of Al_2O_3-(3-x)SrO: xSm^{3+} (x = 0.01, 0.03, 0.06, 0.1, 0.2) glasses is calculated and shown in Figure 9 to investigate the dominant emission color. The CIE chromaticity coordinates (x, y) are presented as (0.59, 0.41), (0.60, 0.40), (0.60, 0.40), (0.59, 0.41) and (0.58, 0.42) for x = 0.01, 0.03, 0.06, 0.1 and 0.2 in Al_2O_3-(3-x)SrO: xSm^{3+}(x = 0.01, 0.03, 0.06, 0.1, 0.2) glasses, respectively, and are located in the orange-reddish region of the visible spectrum. The chromatic color coordinates of the obtained glasses are found to be consistent with other Sm^{3+} doped glasses [15,27,37].

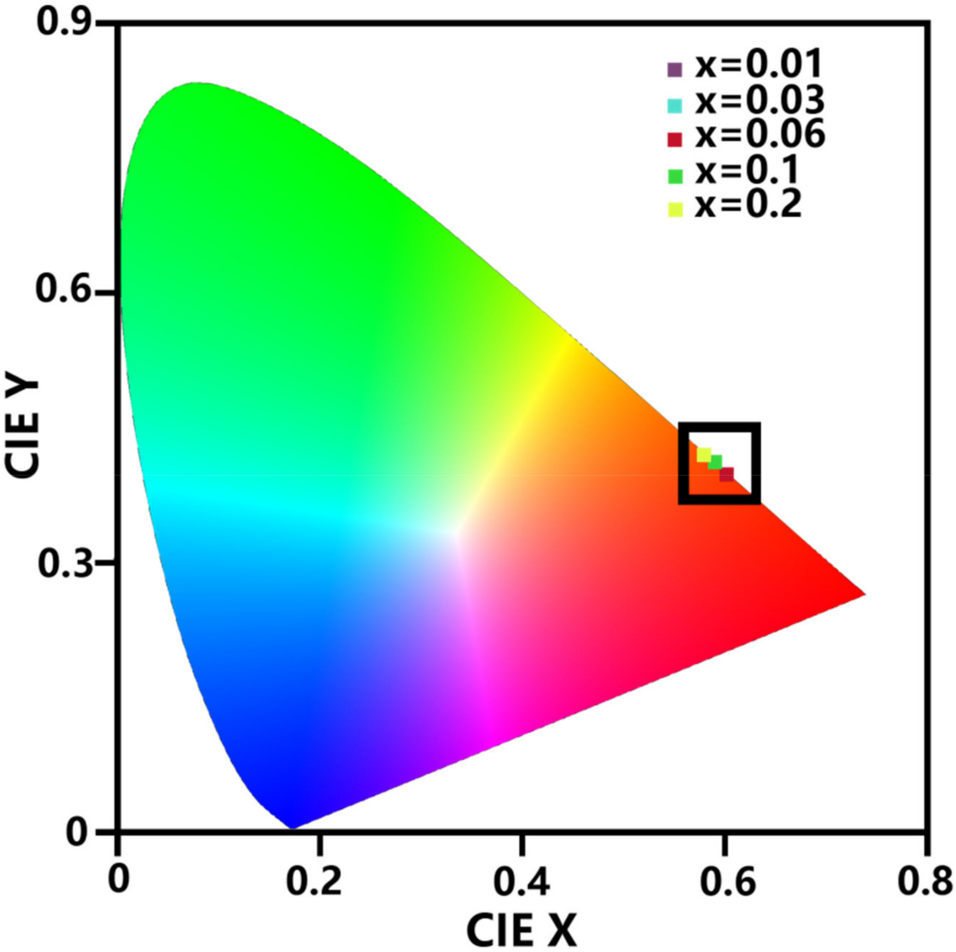

Figure 9. CIE chromaticity of Al_2O_3-(3-x)SrO: xSm^{3+} glasses.

4. Conclusions

Sm^{3+} doped Al_2O_3-(3-x)SrO: xSm^{3+} (x = 0, 0.01, 0.03, 0.06, 0.1, 0.2) transparent glasses with high mechanical hardness were successfully prepared by a containerless process. The excellent glass-forming ability and thermal stability can be detected in these glasses. Elevating the content of Sm^{3+} ions augmented the emissions first and then reduced them when x reached 0.03, verifying the concentration quenching effect. A bright orange-reddish luminescence was observed in Al_2O_3-(3-x)SrO: xSm^{3+} glasses, indicating that these glasses are promising materials for developing visible orange-reddish lasers and smart photoluminescent coating films.

Author Contributions: Data curation, J.Z.; Formal analysis, X.L.; Funding acquisition, P.L., X.Z. and X.Q.; Investigation, P.L. and X.L.; Methodology, J.Z.; Resources, X.Z.; Writing—original draft, P.L. and X.Q. All authors have read and agreed to the published version of the manuscript.

Funding: This work was financially supported by the National Natural Science Foundation of China (No. 51972048) and the Fundamental Research Funds for the Central Universities (No. N2023010, N2123003).

Institutional Review Board Statement: Not applicable.

Informed Consent Statement: Not applicable.

Data Availability Statement: Data sharing is not applicable to this article.

Conflicts of Interest: The authors declare no conflict of interest.

References

1. Roy, J.S.; Messaddeq, Y. Photoluminescence study of Eu^{3+} doped zinc-tungsten-antimonite glasses for red LED applications. *J. Lumin.* **2020**, *228*, 117608. [CrossRef]
2. Subrahmanyam, T.; Gopal, K.R.; Suvarna, R.P.; Jamalaiah, B.C.; Kumar, M.V.V. Luminescent properties of Tb^{3+}-doped TeO_2-WO_3-GeO_2 glasses for green laser applications. *Opt. Mater.* **2018**, *80*, 154–159. [CrossRef]
3. Lakshminarayana, G.; Baki, S.O.; Lira, A.; Kityk, I.V.; Caldiño, U.; Kaky, K.M.; Mahdi, M.A. Structural, thermal and optical investigations of Dy^{3+}-doped B_2O_3-WO_3-ZnO-Li_2O- Na_2O glasses for warm white light emitting applications. *J. Lumin.* **2017**, *186*, 283–300. [CrossRef]
4. Khattab, T.A.; Rehan, M.; Shaheen, Y.H.T.I. Facile development of photoluminescent textile fabric via spray coating of Eu (II)-doped strontium aluminate. *Ind. Eng. Chem. Res.* **2018**, *57*, 11483–11492. [CrossRef]
5. Al-Qahtani, S.D.; Binyaseen, A.M.; Aljuhani, E.; Aljohani, M.; Alzahrani, H.K.; Shah, R.; El-Metwaly, N.M. Production of smart nanocomposite for glass coating toward photochromic and long-persistent photoluminescent smart windows. *Ceram. Int.* **2022**, *48*, 903–912. [CrossRef]
6. Mohan, S.; Kaur, S.; Singh, D.P.; Kaur, P. Structural and luminescence properties of samarium doped lead alumino borate glasses. *Opt. Mater.* **2017**, *73*, 223–233. [CrossRef]
7. Chen, L.; Zhang, Z.; Tian, Y.F.; Fei, M.; He, L.R.; Zhang, P.J.; Zhang, W.H. Origin of the red luminescence in $Sr_3Al_2O_6$: Eu phosphor-from the synergetic effects of Eu^{2+} and Eu^{3+}. *J. Rare Earths* **2017**, *35*, 127–134. [CrossRef]
8. Zhang, X.Y.; Yang, W.C.; Zhang, J.R.; Li, J.S.; Jiang, L.H.; Qi, X.W. High hardnesses of Tm^{3+}-doped La_2O_3-Al_2O_3 luminescent glasses fabricated by containerless solidification. *J. Non-Cryst. Solids* **2019**, *525*, 119599. [CrossRef]
9. Ma, X.G.; Li, X.Y.; Li, J.Q.; Genevois, C.; Ma, B.Q.; Etienne, A.; Wan, C.L.; Véron, E.; Peng, Z.J.; Allix, M. Pressureless glass crystallization of transparent yttrium aluminum garnet-based nanoceramics. *Nat. Commun.* **2018**, *9*, 1175. [CrossRef]
10. Basavapoornima, C.; Linganna, K.; Kesavulu, C.; Ju, S.; Kim, B.; Han, W.-T.; Jayasankar, C. Spectroscopic and pump power dependent upconversion studies of Er^{3+}-doped lead phosphate glasses for photonic applications. *J. Alloys Compd.* **2017**, *699*, 959–968. [CrossRef]
11. Zhang, X.Y.; Zhang, M.; Zhang, J.R.; Li, Y.; Gu, Y.H.; Qi, X.W. Photoluminescence, transmittance and electrical properties of Eu^{3+}-doped Al_2O_3-SrO glasses synthesized by an aerodynamic levitation technique. *J. Lumin.* **2019**, *206*, 79–83. [CrossRef]
12. Devi, C.B.A.; Swapna, K.; Mahamuda, S.; Venkateswarlu, M.; Prasad, M.V.V.K.S.; Reddy, K.S.R.K.; Deopa, N.; Rao, A.S. Spectroscopic studies and lasing potentialities of Sm^{3+} ions doped single alkali and mixed alkali fluoro tungstentellurite glasses. *Opt. Laser Technol.* **2019**, *111*, 176–183. [CrossRef]
13. Jlassi, I.; Mnasri, S.; Elhouichet, H. Concentration dependent spectroscopic behavior of Sm^{3+}-doped sodium fluoro-phosphates glasses for orange and reddish-orange light emitting applications. *J. Lumin.* **2018**, *199*, 516–527. [CrossRef]
14. Kirdsiri, K.; Ramakrishna, R.R.; Damdee, B.; Kim, H.J.; Kaewjaeng, S.; Kothan, S.; Kaewkhao, J. Investigations of optical and luminescence features of Sm^{3+} doped Li_2O-MO-B_2O_3 (M = Mg/Ca/Sr/Ba) glasses mixed with different modifier oxides as an orange light emitting phosphor for WLED's. *J. Alloys Compd.* **2018**, *749*, 197–204. [CrossRef]
15. Vijayakumar, M.; Marimuthu, K.; Sudarsan, V. Concentration dependent spectroscopic behavior of Sm^{3+} doped lead fluoro-borophosphate glasses for laser and LED applications. *J. Alloys Compd.* **2015**, *647*, 209–220. [CrossRef]
16. Deopa, N.; Rao, A.S.; Choudhary, A.; Saini, S.; Navhal, A.; Jayasimhadria, M.; Haranath, D.; Prakash, G.V. Photoluminescence investigations on Sm^{3+} ions doped borate glasses for tricolor w-LEDs and lasers. *Mater. Res. Bull.* **2018**, *100*, 206–212. [CrossRef]
17. Ahmadi, F.; Asgari, A. Spectroscopic investigation of Sm^{3+} doped sulfophosphate glasses for visible photonic applications. *J. Non-Cryst. Solids* **2019**, *505*, 406–413. [CrossRef]
18. Wang, S.Y.; Zhang, H.B.; Wang, T.; Lv, H.M.; Zou, X.Y.; Wei, Y.L.; Hu, W.H.; Su, C.H. Synthesis and luminescence properties of Sm3+ doped molybdate glass ceramic. *J. Alloys Compd.* **2020**, *823*, 153822. [CrossRef]
19. Rudramamba, K.S.; Reddy, D.V.K.; Rao, T.S.; Taherunnisa, S.K.; Veeraiah, N.; Reddy, M.R. Optical properties of Sm^{3+} doped strontium bismuth borosilicate glasses for laser applications. *Opt. Mater.* **2019**, *89*, 68–79. [CrossRef]
20. Zhu, M.G.; Wang, L. Study on the relationship between the melting point the hardness of the alkaline earth metal oxide and the electron structure. *J. Ningbo Univ.* **2004**, *17*, 482–484.
21. Prabhu, N.S.; Hegde, V.; Wagh, A.; Sayyed, M.I.; Agar, O.; Kamath, S.D. Physical, structural and optical properties of Sm^{3+} doped lithium zinc alumino borate glasses. *J. Non-Cryst. Solids* **2019**, *515*, 116–124. [CrossRef]
22. Li, P.F.; Qi, X.W.; Wang, L.M. A comprehensive study of lead telluride (PbTe)-based amorphous alloys: Glass formation and thermoelectric properties. *J. Non-Cryst. Solids* **2021**, *571*, 121057. [CrossRef]
23. Zhang, M.H.; Wen, H.Q.; Pan, X.H.; Yu, J.D.; Shao, H.; Tang, M.B.; Gai, L.J.; Ai, F. Study on novel high refractive index La_2O_3-Lu_2O_3-TiO_2 glasses prepared by aerodynamic levitation method. *Mater. Lett.* **2018**, *222*, 5–7. [CrossRef]
24. Rasool, S.N.; Moorthy, L.R.; Jayasankar, C.K. Spectroscopic Investigation of Sm^{3+} doped phosphate based glasses for reddish-orange emission. *Opt. Commun.* **2013**, *311*, 156–162. [CrossRef]
25. Yamusa, Y.A.; Hussin, R.; Shamsuri, W.N.W. Physical, optical and radiative properties of $CaSO_4$-B_2O_3-P_2O_5 glasses doped with Sm3+ ions. *Chin. J. Phys.* **2018**, *56*, 932–943. [CrossRef]
26. Mohan, S.; Kaur, S.; Kaur, P.; Singh, D.P. Spectroscopic investigations of Sm^{3+}-doped lead alumino-borate glasses containing zinc, lithium and barium oxides. *J. Alloys Compd.* **2018**, *763*, 486–495. [CrossRef]

27. Shamshad, L.; Ali, N.; Kaewkhao, J.; Rooh, G.; Ahmad, T.; Zaman, F. Luminescence characterization of Sm^{3+}-doped sodium potassium borate glasses for laser application. *J. Alloys Compd.* **2018**, *766*, 828–840. [CrossRef]
28. Boehm, L.; Reisfeld, R.; Spector, N. Optical transitions of Sm^{3+} in oxide glasses. *J. Solid State Chem.* **1979**, *28*, 75–78. [CrossRef]
29. Jorgensen, C.K. *Oxidation Numbers and Oxidation States*; Springer Science & Business Media: New York, NY, USA, 1969; Volume 6, pp. 72–140.
30. Shamshad, L.; Rooh, G.; Kirdsiri, K.; Srisittipokakun, N.; Damdee, B.; Kim, H.J. Photoluminescence and white light generation behavior of lithium gadolinium silicoborate glasses. *J. Alloys Compd.* **2017**, *695*, 2347–2355. [CrossRef]
31. Carnall, W.T.; Fields, P.R.; Rajnak, K. Electronic energy levels in the trivalent lanthanide aquo ions. I. Pr^{3+}, Nd^{3+}, Pm^{3+}, Sm^{3+}, Dy^{3+}, Ho^{3+}, Er^{3+}, Tm^{3+}. *J. Chem. Phys.* **1968**, *49*, 4424–4442. [CrossRef]
32. Sreedhar, V.B.; Basavapoornima, C.; Jayasankar, C.K. Spectroscopic and fluorescence properties of Sm^{3+} doped zinc fluorophosphate glasses. *J. Rare Earths* **2014**, *32*, 918–926. [CrossRef]
33. Swapna, K.; Mahamuda, S.; Rao, A.S.; Shakya, S.; Sasikala, T.; Haranath, D.; Prakash, G.V. Optical studies of Sm^{3+} ions doped zinc alumino bismuth borate glasses. *Spectrochim. Acta A* **2014**, *125*, 53–60. [CrossRef]
34. Talewar, R.A.; Mahamuda, S.; Swapna, K.; Venkateswarlu, M.; Rao, A.S. Spectroscopic studies of Sm^{3+} ions doped alkaline-earth chloro borate glasses for visible photonic applications. *Mater. Res. Bull.* **2018**, *105*, 45–54. [CrossRef]
35. Basavapoornima, C.; Jayasankar, C.K. Spectroscopic and photoluminescence properties of Sm^{3+} ions in Pb-K-Al-Na phosphate glasses for efficient visible lasers. *J. Lumin.* **2014**, *153*, 233–241. [CrossRef]
36. Liang, X.; Yang, Y.; Zhu, C.; Yuan, S.; Chen, G. Luminescence properties of Tb^{3+}-Sm^{3+} codoped glasses for white light emitting diodes. *Appl. Phys. Lett.* **2007**, *91*, 091104. [CrossRef]
37. Mariyappan, M.; Arunkumar, S.; Marimuthu, K. Concentration effect on the structural and spectroscopic investigations of Sm^{3+} ions doped B_2O_3-Bi_2O_3-CaF_2-Na_2O glasses. *J. Lumin.* **2018**, *196*, 151–160. [CrossRef]
38. Suthanthirakumar, P.; Arunkumar, S.; Marimuthu, K. Spectroscopic properties and excited state dynamics of Sm^{3+} ions in zinc telluro-flfluoroborate glasses. *J. Lumin.* **2018**, *202*, 289–300. [CrossRef]
39. Puchalska, M.; Zych, E. The effffect of charge compensation by means of Na^+ ions on the luminescence behavior of Sm^{3+}-doped $CaAl_4O_7$ phosphor. *J. Lumin.* **2012**, *132*, 826–831. [CrossRef]
40. Min, X.; Fang, M.H.; Huang, Z.H.; Liu, Y.A.; Tang, C.; Zhu, H.K.; Wu, X.W. Preparation and luminescent properties of orange reddish emitting phosphor $LaMgAl_{11}O_{19}$:Sm^{3+}. *Opt. Mater.* **2014**, *37*, 110–114. [CrossRef]